Journal of Metals, Materials and Minerals, 35(1), e2153, 2025

Enhancement of cell viability of the (Ba,Ca)(Zr,Ti)O_3 and hydroxyapatite composites for bone-repair applications

Jirapa TANGSRITRAKUL[1,*], Manita BOONCHOO[1], Piyanan BOONPHAYAK[2,3], Paweena UPPANAN[4], and Pakkanun KAEWKONG[4]

[1] *Faculty of Science and Technology, Thammasat University, Pathum Thani 12120, Thailand*
[2] *Department of Industrial Engineering, Engineering Faculty, Naresuan University*
[3] *Center of Excellence in Biomaterials, Faculty of Science, Naresuan University, Phitsanulok 65000, Thailand*
[4] *National Metal and Materials Technology Center, Thailand Science Park, Pathum Thani 12120, Thailand*

***Corresponding author e-mail**: tjirapa@tu.ac.th

Received date:
15 September 2024
Revised date:
21 November 2024
Accepted date:
18 December 2024

Keywords:
Bone-tissue engineering;
Bone-repair applications;
Lead-free piezoceramics;
Barium titanate;
Hydroxyapatite

Abstract

In this work, the influence of hydroxyapatite (HA) addition to the calcium/zirconium-doped barium titanate (BCZT) piezoceramic was investigated to evaluate its potential for bone-repair applications. The relationship between the physical, electrical, and biological properties of the (100-x)BCZT-(x)HA composite was observed via various techniques. The HA powder was synthesized via precipitation method, whereas the BCZT powder was produced by solid-state reaction to prepare the (100-x)BCZT-(x)HA composites, where x = 0 wt% to 50 wt%. The results showed that the dielectric, ferroelectric, and piezoelectric properties of the (100-x)BCZT-(x)HA composites decreased dramatically as introducing HA into BCZT due to the occurrence of secondary phases from the reactivity between BCZT and HA during sintering. However, although the addition of 10wt%HA into BCZT caused a significant drop of its electrical properties, the enhancement of MC3T3-E1 cell viability was found. Moreover, this work demonstrates for the first time that the number of viable cells observed in the poled 90BCZT-10HA ceramics was significantly higher than that observed in the unpoled BCZT ceramics. These results suggest that the BCZT-HA composite has potential for use in bone-repair applications.

1. Introduction

Piezoelectric effect was observed in Femur or thigh bone of human reported by Fukuda *et al.* [1]. They found that the configuration of collagen fibers in bone played a crucial role on the presence of piezoelectricity in both direct effect (stress induced electric potential) and converse effect (strain developed under electric field). The piezo-electric effect was later observed in similar results in the dentine studied by Braden; however, it was not found in the enamel because the enamel does not contain collagen [2]. Additionally, the generation of electric charge under mechanical stress induces a biological response which initiates the development of bone growth and healing [3,4]. These findings suggested that lead-free piezoelectric materials may also be considered as a promising candidate for bone-repair and regeneration applications.

Barium Titanate (BT) is a lead-free piezoceramic used in early state for implant test in dogs, which has provided reliable data to support it as a good biocompatibility and feasibility material for bone replacement [5]. Moreover, another possibility was observed in the calcium/zirconium-doped barium titanate (BCZT) which recently showed non-cytotoxicity as well as large piezoelectric coefficient d_{33} [6,7]. However, Chen *et al.* found the enhancement of MC3T3 cell growth on the poled surface of potassium sodium niobate (KNN) piezoceramic in comparison to the unpoled KNN, which leads to another potential material that can be utilizing for bone-tissue engineering [8]. Similarly, the bioactivity of the poled and unpoled bismuth sodium titanate (BNT) piezoceramic was investigated by the immersion of the samples into Hank's solution, and it was found that bone-like apatite grew on poled BNT ceramic quicker than unpoled BNT [9]. These observations indicated that various lead-free piezoelectric materials were suitable for bone-tissue engineering. Moreover, the presence of surface charges on piezoelectric materials provided an acceleration of the biological response.

In terms of the well-known hydroxyapatite (HA) that has been widely used for bone grafts, fillers and as coatings for metal implants, the generation of polarization of HA can be induced through the application of a high DC electric field (around 1 $kV{\cdot}cm^{-1}$ to 10 $kV{\cdot}cm^{-1}$) at elevated temperature (above 200°C) to reorient protons in OH^- columnar structure. Consequently, the polarization of the material was able to provide a beneficial impact on the biological activity in the polarized HA surface [3,10,11]. In addition, various *In-vivo* and *In-vitro* studies confirmed that the enhancement of cell adhesion, osteobonding, and new bone formation was observed on the polarized HA surface with negative charges compared to the non-polarized surface [12-14]. This was attributed to the adsorption of elements that included Ca^{2+} cations and the negative surface charges of polarized

HA. This interaction therefore enhanced the formation of a bone-like crystal layer, which encouraged the adsorption of protein and cell attachment [13].

Hydroxyapatite is commonly used for bone-tissue engineering because its chemical composition is similar to the bone tissue, while piezoelectric materials can generate electric charges under stress. The combination of these materials is used to enhance the biological performance of the healing of bone tissue. Equally important, this piezoceramic-hydroxyapatite composite process also evaluated the potential for bone-repair applications [15-19]. Several studies focused on the characterization of the Barium Titanate-Hydroxyapatite composites [16,17,19,20]. It has been reported that the biocompatibility and bone-induction activity of BT-HA ceramics were better than the pure HA. Moreover, the application of cyclic loading on the BT-HA ceramics during the co-culturing process of osteoblast cells could significantly enhance cell number as a result of the presence of electrical stimulation from piezoelectric properties in $BaTiO_3$ ceramic [17]. However, reactivity between BT and HA during the sintering process at a high temperature provided evidence of $Ba_3(PO_4)_2$ secondary phase, which was dissolved and released Ba^{2+} ions in the culture media that consequently dropped cell viability [19].

Alternatively, the introduction of the β-tricalcium phosphate (β-TCP) bioactive material to the strontium doped barium titanate (BST) piezoelectric material was fabricated using a 3D printing to create the scaffold of the BST/β-TCP composite, which presented the highest level of biological and mechanical properties at the 60% BST/40% β-TCP composition [18]. In addition, Ozcelik found the improvement of osteoblast adhesion observed in the tricalcium phosphate/barium titanate (TCP/BT) and hydroxyapatite/barium titanate (HA/BT) compared to pure HA and TCP [20]. Moreover, the synthesis of injectable barium titanate-modified calcium phosphate bone cement (CPC) was successful while also exhibiting good compressive strength, injectability, bioactivity, and biocompatibility that were suitable for orthopedic and spinal-fusion applications [21].

The number of publications on piezoelectric materials for bone-tissue engineering has rapidly increased in the last few years, as reported by Tandon *et al.* [22]. This implies that the utilization of piezoelectric materials for bone-repair applications is a promising procedure; yet still challenging. To date, several studies have attempted to evaluate the impact of HA addition into BT on the biological performance for bone-tissue engineering, as mentioned earlier. Conversely, it has been demonstrated that the calcium/zirconium-doped barium titanate (BCZT) showed excellent piezoelectric coefficient (d_{33} ~ 620 pC N^{-1}), significantly larger than pure BT and also non-toxic [7]. Additionally, there is very little published research on the investigation of HA-BCZT composite and its potential for bone-repair application [15]. Therefore, this work aims to explore the influence of HA addition into BCZT piezoceramic on the relationship between physical, electrical, and biological properties needed to evaluate the future potential usage for bone healing and regeneration.

2. Experimental procedures

Pure hydroxyapatite ($Ca_{10}(PO_6)_4(OH)_2$ or HA) was prepared via the precipitation method from aqueous solutions using analytical grade $Ca(NO_3)_2{\cdot}4H_2O$ (≥99.0%) and $(NH_4)_2HPO_4$ (≥98%) obtained by Sigma Aldrich as precursors. In addition, the precursors maintained the experimental ratio of Ca/P at 1.67. The mixture was controlled at a pH of 10 using a NH_3 solution. After aging the mixture at room temperature overnight, it was filtered, and washed with deionization water until a pH of 7 was reached. Lastly, the product was dried in an oven at 110°C for overnight. On the other hand, the calcium/zirconium-doped barium titanate ($Ba_{0.85}Ca_{0.15}Ti_{0.9}Zr_{0.1}O_3$ or BCZT) was produced via a solid-state reaction using $BaCO_3$ (99.0%), $CaCO_3$ (99.0%), TiO_2 (99.0%) and ZrO_2 (99.0%) as raw materials. Then, all precursors were weighed in stoichiometric amounts prior to ball milling for 24 h and followed by drying in an oven at 90°C for overnight. The mixed powder was then calcined at 1250°C for 3 h at a heating rate of 5°C·min^{-1}.

For preparation of the (100-x)BCZT-(x)HA composites, HA and BCZT powders were mixed at different compositions where x = 0, 10, 30, and 50wt% of HA (denoted as BCZT, 90BCZT-10HA, 70BCZT-30HA, and 50BCZT-50HA, respectively) using ball mill for 24 h and dried at 90°C for overnight. Then, the (100-x)BCZT-(x)HA mixed powder was weighed for 0.3 g and mixed with 3 wt% Polyvinyl alcohol (PVA) as a binder before uniaxial pressing at ~ 95 MPa for 30 sec into a disc shape with diameter of ~13 mm and thickness of ~2 mm. Next, the green samples were stacked in an alumina crucible and sintered for 3 h at 1400°C in order to achieve the BCZT ceramic and at 1250°C for the (100-x)BCZT-(x)HA ceramics with a heating rate of 5°C·min^{-1}.

Phase formation of the (100-x)BCZT-(x)HA ceramics was analyzed by X-ray diffractometer (XRD: Bruker AXS Model D8 Advance, Germany) over the range of 2θ between 20° to 60°. For microstructural observations, the (100-x)BCZT-(x)HA ceramics were mounted using epoxy resin and followed by grinding using Silicon Carbide (SiC) papers: P400, P800, P1200, and then polished the surface with a 6 μm, 1 μm, and 0.25 μm diamond paste and colloidal silica suspension in the final step, respectively. Afterward, the polished (100-x)BCZT-(x)HA ceramics were coated with gold by sputtering. Field Emission Scanning Electron Microscope (FE-SEM: JEOL JSM7800F, JAPAN) with an accelerating voltage of 15kV was employed to observe the cross-sectional microstructure of the (100-x)BCZT-(x)HA ceramics. In addition, the chemical analysis was examined using an energy-dispersive X-ray spectrometer (EDS: Oxford X-Max 20, UK). The average grain size was investigated using the linear intercept method. For density and porosity observations, the bulk density (ρ_s) of the (100-x)BCZT-(x)HA ceramics was measured using the Archimedes method, whereas Equation (1) was employed to calculate the theoretical density (ρ_t) of the (100-x)BCZT-(x)HA composites [23].

$$\frac{1}{\rho_t} = \frac{(1-x)}{\rho_1} + \frac{x}{\rho_2} \quad (1)$$

Where ρ_1 and ρ_2 are theoretical density of BCZT (5.75 g·cm^{-3}) and HA (3.17 g·cm^{-3}), respectively, and x is HA content. In addition, the percentage of porosity (%P) for the (100-x)BCZT-(x)HA ceramics was determined using Equation (2) [19].

$$\%\,P = 100\left(1 - \frac{\rho_s}{\rho_t}\right) \quad (2)$$

For electrical measurements, both parallel surfaces of the (100-x) BCZT-(x)HA ceramic discs were polished with a P800 SiC paper

to obtain thickness of ~ 1 mm before applying silver electrode (Heraeus PCC11889, Germany) and firing at 550°C for 1 h. The frequency and temperature dependences of dielectric properties were measured using an LCR meter (Agilent E4980A precision LCR meter) over a frequency range between 10^2 Hz to 10^6 Hz and temperature between room temperature to 150°C. The field-dependent polarization (P-E) hysteresis loop and field-dependent strain (s-E) butterfly loop were examined under the maximum electric field of ±30 kV cm^{-1} at a frequency of 2 Hz using the Precision Premier II ferroelectric tester (RADIANT Technologies, inc., US).

Additionally, a contact angle measurement was employed to evaluate surface property for the unpoled (100-x)BCZT-(x)HA ceramics that were smoothed with P800 SiC paper. The surfaces were then cleaned with ethanol before testing was carried out using the static sessile drop technique via a contact angle analyser (Biolin Scientific, 100 Theta Lite Optical Tensiometer). On the other hand, the influences of a polarized surface on the negative charges regarding the *in vitro* biocompatibility was also investigated related to the BCZT and 90BCZT-10HA ceramics in this work. The poling process was done by increasing and decreasing the applied field from 0 kV·cm^{-1} to 20 kV·cm^{-1} at a frequency of 2 Hz for 2 cycles on the BCZT and 90BCZT-10HA ceramics without electrode to avoid the presence of impurities on the samples. This poling process was carried out prior to cell culture being placed on the negative charges poled surface of the BCZT and 90BCZT-10HA ceramics in comparison with the unpoled ceramics.

The *in vitro* biocompatibility of unpoled and poled BCZT and 90BCZT-10HA ceramics was evaluated regarding cell viability and morphology using MC3T3-E1 subclone 4 pre-osteoblasts (ATCC® CRL-2593™). In brief, the samples were sterilized with UV-light for 2 h on each side. The sterilized samples were placed in 24-well plates and then MC3T3-E1 cells were seeded onto each sample at a concentration of 50,000 cells/sample. The cell-seeded samples were then cultured in a culture medium (α-minimum essential medium or α-MEM; Gibco, USA) supplemented with 10% fetal bovine serum (FBS; Gibco, USA), and 1% antibiotic-antimycotic solution (Gibco, USA) at 37°C in a humidified atmosphere of 5%CO_2 in air. After 24 h of incubation, the cell viability was examined using live/dead staining. The cell-seeded samples were washed twice in phosphate-buffered saline (PBS) and stained using a Live/Dead viability/cytotoxicity kit (Molecular Probes, Invitrogen) according to the manufacturer's recommendations. Cell viability was also evaluated using the Alamar Blue assay. The cell-seeded samples were incubated in the culture medium containing 0.5 mM resazurin (Sigma-Aldrich) for 4 h at 37°C. The fluorescence intensity was measured at ex/em 530 nm/590 nm using a microplate reader (VICTORTM X4, Perkin Elmer, Waltham, MA). Each sample was normalized to the control (polystyrene wells with cells). Data were reported as the mean percentage of viability (n = 3).

3. Results and discussion

3.1 Phase formation

XRD profiles of the (100-x)BCZT-(x)HA composite sintered at 1400°C for pure BCZT and at 1250°C for 90BCZT-10HA, 70BCZT-30HA, and 50BCZT-50HA were investigated, as shown in Figure 1(a). The perovskite structure (PDF: 01-082-2813) was observed in the pure BCZT ceramics without secondary phases. As introducing HA into BCZT for 10 wt%, the perovskite structure of BCZT was still founded in the 90BCZT-10HA ceramic with small amount of HA reflections. However, the reflections of secondary phases including α-TCP (PDF: 00-009-0348), $CaTiO_3$ (PDF: 00-042-0423), and $Ba_3Ca_3(PO_4)_2$ (PDF: 00-024-0091) were also observed in the XRD profile of the 90BCZT-10HA ceramic. This implies that the stability of HA and BCZT phases reduced after introducing 10 wt% HA into BCZT and reacted at high temperature during sintering process. Furthermore, it was found in Figure 1(b) that the major peak of the BCZT phase slightly shifted to higher 2θ values and became broader as adding 10 wt% HA into BCZT. This indicates that some Ca^{2+} (134 pm) from HA may partially substitute into the Ba^{2+} (164 pm) site of the BCZT perovskite structure, leading to a slight decrease in the crystal lattice as HA content increases [24].

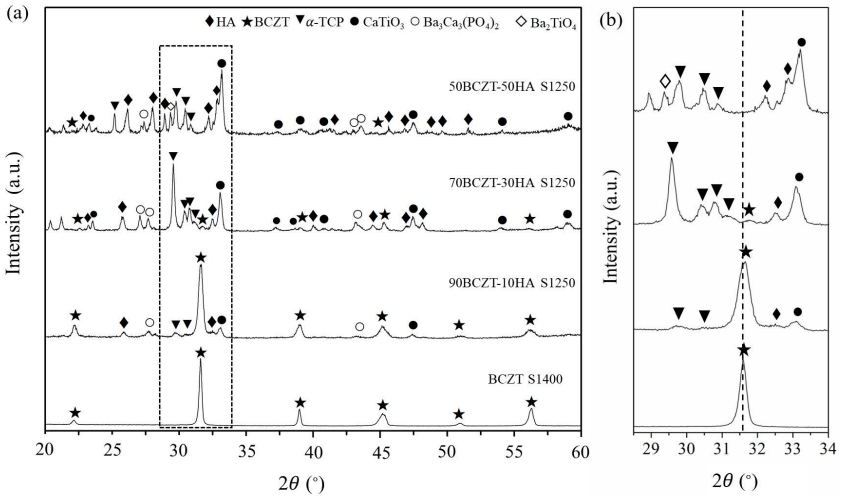

Figure 1. (a) XRD profiles of pure BCZT ceramic sintered at 1400°C for 3 h and 90BCZT-10HA, 70BCZT-30HA, and 50BCZT-50HA sintered at 1250°C for 3 h, showing the occurrence of secondary phases observed in the (100-x)BCZT-(x)HA composite, (b) The enlargement of the XRD profiles in the 2θ range between 28.5° and 34°, presenting the BCZT peak shifting to higher 2θ values as HA content increased.

When HA content was increased to 30 wt%, the intensity of the XRD peaks for the BCZT phase dropped dramatically, while the reflections of secondary phases (α-TCP, $CaTiO_3$, and $Ba_3Ca_3(PO_4)_2$) became stronger, as seen in Figure 1(b). This can be explained by the fact that the content of HA addition for the 70BCZT-30HA ceramic was higher than the 90BCZT-10HA ceramic, resulting in a strong formation of reaction products. Consequently, the residue of unreacted BCZT phase observed in the XRD profile of 70BCZT-30HA ceramic was extremely lower than that observed in the 90BCZT-10HA ceramic. In contrast, as HA content increased to 30 wt%, the presence of unreacted HA, α-TCP, and $CaTiO_3$ phase in the 70BCZT-30HA ceramic was gradually higher than that observed in the 90BCZT-10HA ceramic, since the intensity of the major peak for HA (occurring at ~ 32.5°), α-TCP (occurring at ~ 29.5°), and $CaTiO_3$ phase (occurring at ~ 33°) increased moderately, as shown in Figure 1(b).

Conversely, as HA content was further increased to 50 wt%, the unreacted BCZT phase became difficult to identify, but an increase in the intensity of the unreacted HA and $CaTiO_3$ peak was found in the XRD profile of 50BCZT-50HA ceramic. Moreover, a gradual drop in the intensity of the α-TCP was observed in the XRD profile of the 50BCZT-50HA ceramic, accompanied by the formation of an additional Ba_2TiO_4 secondary phase (PDF: 00-008-0277), as seen in Figure 1(b). These results indicated that the reactivity between BCZT and HA occurred dominantly in the 50BCZT-50HA ceramic. As a result, the occurrence of various secondary phases (α-TCP, $CaTiO_3$, $Ba_3Ca_3(PO_4)_2$, and Ba_2TiO_4) was mainly observed in this composition.

Correspondingly, Ozcelik found that the reactivity between HA and BT was observed when sintering temperature increased to 900°C, leading to the presence of $CaTiO_3$ and Ba_2TiO_4 secondary phases [20]. In this work, the formation of all secondary phases observed in the (100-x)BCZT-(x)HA composite may occur when temperature increased to 1250°C, leading to the occurrence of liquid phase that partially dissolved the phosphate and titanate phases and consequently recrystallized into the secondary phases during cooling [19].

3.2 Microstructural observation

Figure 2 illustrates the polished cross-sectional microstructure and EDS analysis of the BCZT, 90BCZT-10HA, 70BCZT-30HA, and 50BCZT-50HA ceramics. It was found that the BCZT ceramic sintered at 1400°C for 3 h showed homogeneous microstructure with average grain size of 6.44 ± 0.79 µm. In contrast, the addition of HA into BCZT ceramic caused the occurrence of chemical heterogeneity with a dramatic drop of the average grain size compared to the pure BCZT ceramic. After adding 10 wt% of HA into BCZT, the average grain size of 0.50 ± 0.14 µm was observed in the 90BCZT-10HA ceramic, see in Figure 2(c). However, the grain size slightly increased from 0.65 ± 0.06 µm to 1.02 ± 0.24 µm as the HA content increased from 30 wt% to 50 wt%, as seen in Figure 2(e) and Figure 2(g), respectively. Moreover, the (100-x)BCZT-(x)HA composites showed more porosity than that observed in the pure BCZT ceramic. The increase of grain size and porosity with increasing HA content may attribute to the occurrence of reactivity between BCZT and HA during sintering, leading to the presence of low-melting-point glassy material and the release of vapor or gas that consequently caused grain growth and inhibited the sinterability of the (100-x)BCZT-(x)HA composites [20].

Furthermore, chemical composition of the BCZT, 90BCZT-10HA, 70BCZT-30HA, and 50BCZT-50HA ceramics was evaluated using EDS analysis, presented in Figure 2(b), Figure 2(d), Figure 2(f), and Figure 2(h), respectively. All elements of the BCZT ceramic were observed in the homogenous microstructure, see in Figure 2(b). Conversely, adding HA into BCZT, phase contrast were clearly visible in all (100-x)BCZT-(x)HA composites, which indicated that there was an occurrence of chemical segregation. EDS analysis was employed to determine the chemical composition in the three different areas, that were labelled as spectrum 1, 2, and 3, in the microstructure of 90BCZT-10HA, 70BCZT-30HA and 50BCZT-50HA composites, shown in Figure 2(d), Figure 2(f), and Figure 2 (h), respectively. It was found that the amounts of Ca, Ti and O were present at an exceedingly high level in spectrum 1 (dark area) for the 90BCZT-10HA and 70BCZT-30HA composites, while the 50BCZT-50HA composite showed a large amount of Ca, P and O in spectrum 1. This implies that the secondary phase of $CaTiO_3$ and TCP or the HA phase may occur in the dark area of the microstructure for the (100-x)BCZT-(x)HA composites.

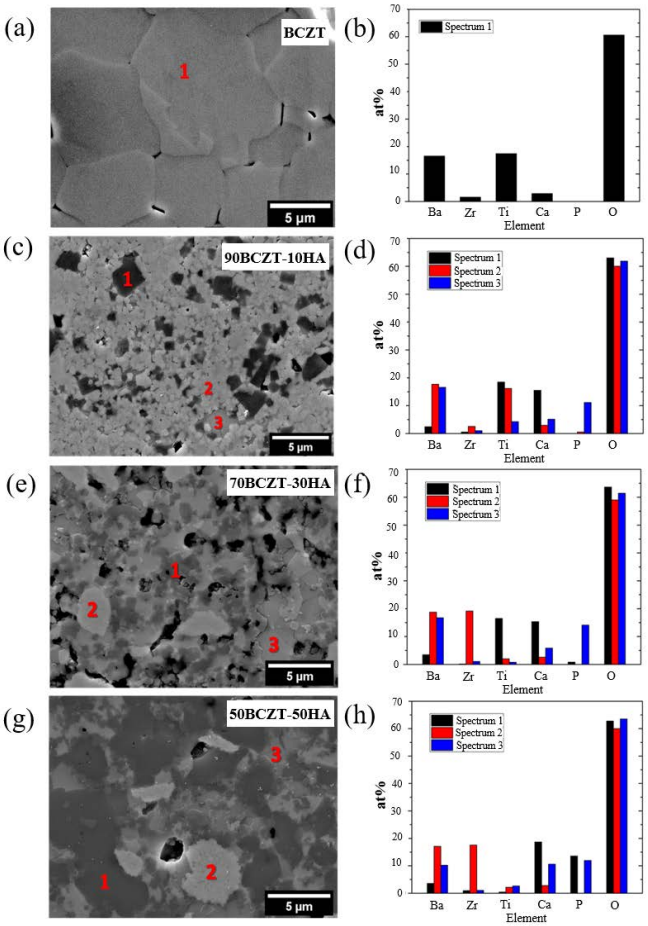

Figure 2. Cross-sectional microstructure and EDS analysis of (a-b) BCZT ceramic sintered at 1400°C for 3 h, (c-d) 90BCZT-10HA, (e-f) 70BCZT-10HA, and (g-h) 50BCZT-50HA ceramics sintered at 1250°C for 3 h, indicating that chemical heterogeneity was observed in the BCZT-HA ceramics.

In contrast, the EDS results of spectrum 2 (bright area 1) revealed that there were large amounts of Ba, Ti and O; yet, there were small amounts of Ca and Zr that were observed in the 90BCZT-10HA composite, which corresponds to the BCZT phase. However, the 70BCZT-30HA and 50BCZT-50HA composites showed the amount of observed Zr in spectrum 2 higher than that found in the 90BCZT-10HA composite; whereas, the traces of P were not detected. This is possibly due to the EDS spectra of P K_α and Zr L_α overlap in the problem region of ~2 keV, which indicated limitations related to peak identification [25]. In addition, the chemical compositions of spectrum 3 (bright area 2) showed a high content of Ba, Ca, P, and O which was consistent with the observed $Ba_3Ca_3(PO_4)_2$ secondary phase in XRD profiles for all compositions of the (100-x)BCZT-(x)HA composites.

3.3 Density and porosity

Bulk density, theoretical density, and porosity percent were determined for the (100-x)BCZT-(x)HA composite, presented in Figure 3. Since the theoretical density of pure BCZT (5.75 g·cm^{-3}) is higher than pure HA (3.17 g·cm^{-3}), the addition of HA into BCZT caused a gradual drop of theoretical density of the (100-x)BCZT-(x)HA ceramics with increasing HA content. In this work, the observed bulk density of the BCZT ceramic sintered at 1400°C for 3 h showed the highest value of 5.64 ± 0.29 g·cm^{-3}. As adding HA into BCZT ceramic from 10 wt% to 50 wt% and sintered at 1250°C for 3 h, the observed bulk density of the 90BCZT-10HA, 70BCZT-30HA, and 50BCZT-50HA ceramics gradually decreased from 5.01 ± 0.09 g·cm^{-3} to 3.75 ± 0.06 g·cm^{-3} when increasing HA amount. Note that the relative density of the (100-x)BCZT-(x)HA composite was observed above 90% in all compositions. Furthermore, the percentage of porosity increased as introducing HA into BCZT ceramics, which corresponded to the observed pores in the microstructure of the (100-x)BCZT-(x)HA composites, as seen earlier in Figure 2. Park *et al.* reported that the increase of porosity can improve the occurrence of bone ingrowth into the pores, leading to the enhancement of biocompatibility [5].

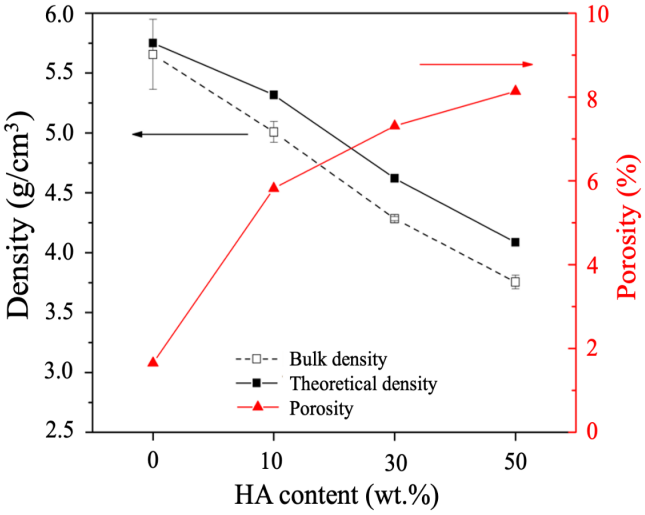

Figure 3. Comparison of bulk density, theoretical density, and porosity percent as a function of HA content for the (100-x)BCZT-(x)HA composites.

3.4 Electrical properties

3.4.1 Dielectric properties

Figure 4 presents the frequency dependence of dielectric permittivity (ε_r) and loss tangent (tan δ) for the (100-x)BCZT-(x)HA ceramics measured at room temperature with a frequency range of 10^2 Hz to 10^6 Hz. It was found that the highest ε_r of 2804 was observed in the pure BCZT ceramic with a tan δ of 0.03 at a frequency of 10^2 Hz. However, as frequency increased to 10^6 Hz, a slight decrease of ε_r from 2804 to 2484 was found for the BCZT ceramic, indicating a gradual drop of polarization response when increasing frequency of the applied field [26].

Surprisingly, the addition of 10 wt% HA into BCZT caused a dramatic drop of ε_r to 688 (at 10^2 Hz), despite the majority phase of the BCZT being present in the XRD profile. This observation reflects the reduction of polarization (negative and positive charges separation) presenting under the application of electric field [27]. It is possible that the observed secondary phases in combination to a dramatic drop of grain size play a key role on the drastic decrease of polarization in the 90BCZT-10HA ceramic. Since chemical heterogeneity and grain boundary can hinder the movement of space charge under the applied field in the polarization process, the observed ε_r dropped significantly. Note that this impact will also be found on the significant drop of ferroelectric and piezoelectric properties, as described later in section 3.4.2 and 3.4.3.

As HA content increased from 30 wt% to 50 wt%, the ε_r (at 10^2 Hz) gradually decreased from 521 to 35 because the amount of secondary phases increased and became the majority phases for the 70BCZT-3HA and 50BCZT-50HA ceramics, respectively. In contrast, the tan δ as a function of frequency for the BCZT, 90BCZT-10HA, and 70BCZT-HA ceramics were not different significantly except for the 50BCZT-50HA composite that showed a noticeable high of tan δ, as seen in Figure 4(b). This suggested that the secondary phases strongly inhibited charge movement in the 50BCZT-50HA composite, resulting in a significant rise of dielectric loss.

The temperature dependence of ε_r and tan δ for the (100-x)BCZT-(x)HA ceramics measured at 10 kHz with temperature range of room temperature to 150°C was also investigated to determine the ferroelectric-paraelectric phase transition temperature or Curie temperature (T_C), illustrated in Figure 5 [28]. For the pure BCZT, the anomaly changes of ε_r and tan δ were observed at T_C ~ 92°C, as seen in Figure 5(a-b). However, the presence of T_C disappears when introducing HA into the BCZT from 10 wt% to 50 wt%, as shown in Figure 5(c-d). Moreover, the value of ε_r gradually decreased with increasing temperature to 150°C for the 90BCZT-10HA and 70BCZT-HA ceramics, while the stable ε_r–T relationship was observed in the 50BCZT-50HA ceramic. These observations are contrary to the observed ε_r–T result for the BT-HA composite, which reported that the addition of 25 wt% HA into the BT ceramic still showed T_C at temperature around 116°C to 126°C [16]. Furthermore, the observed tan δ of the 90BCZT-10HA, 70BCZT-HA, and 50BCZT-50HA ceramics rises gradually with increasing temperature to 150°C. This could be attributed to the enhancement of free charge carrier occurred by temperature that consequently led to the presence of high conductivity and high loss tangent in the samples [16,29].

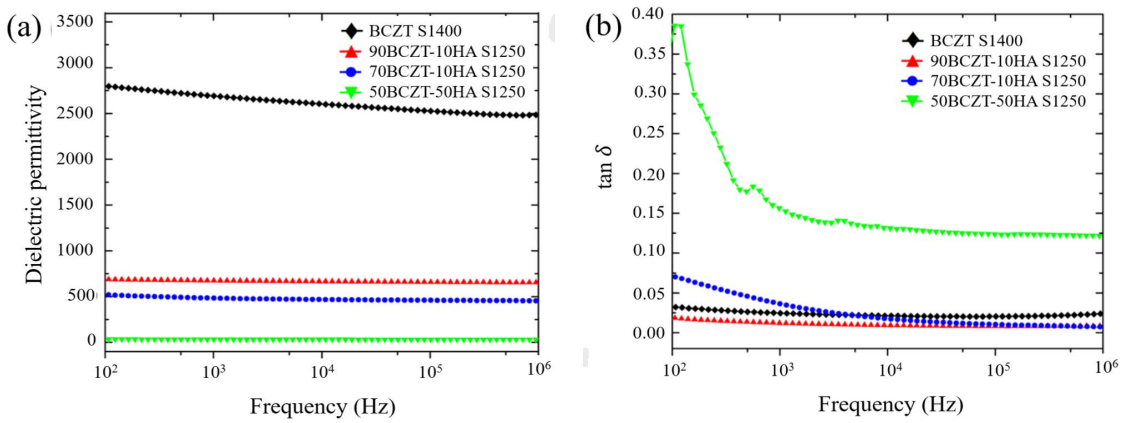

Figure 4. Frequency dependence of (a) dielectric permittivity, and (b) tan δ of the (100-x)BCZT-(x)HA composites measured at room temperature.

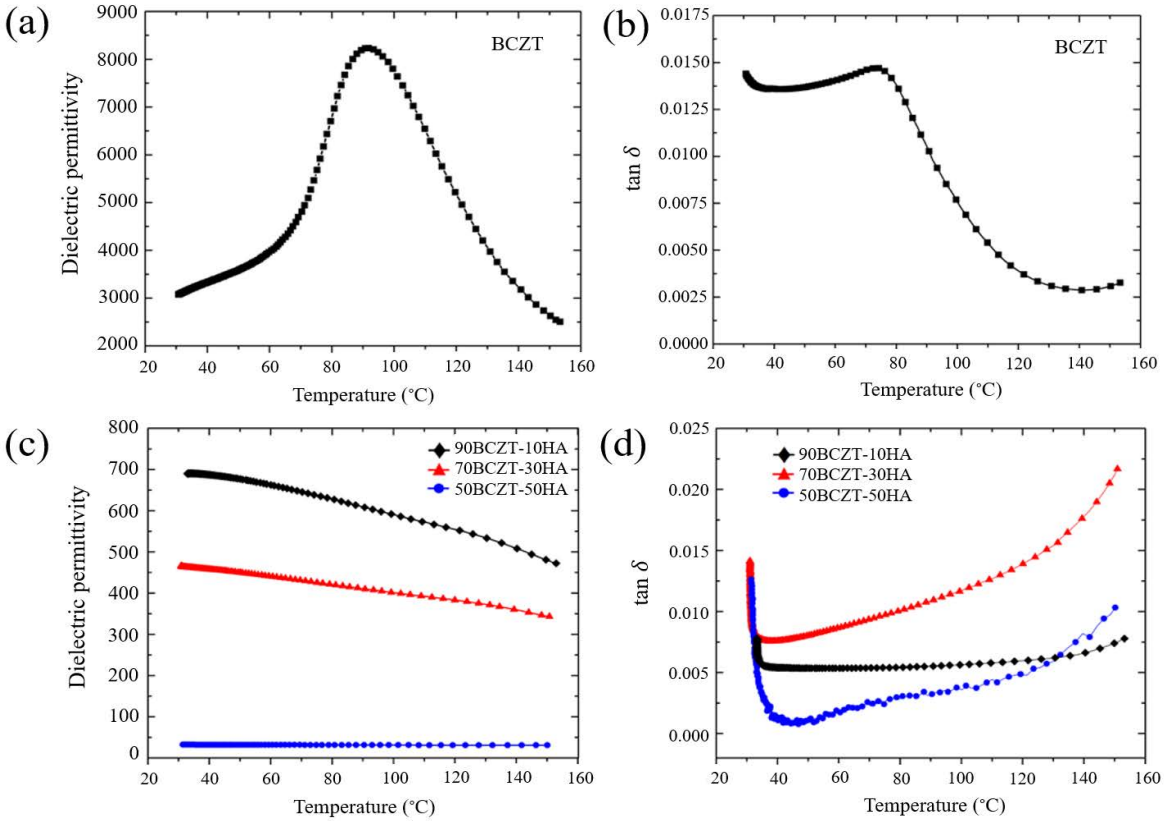

Figure 5. Temperature dependence of dielectric permittivity and loss tangent measured at 10kHz of (a-b) the pure BCZT ceramic, and (c-d) the (100-x)BCZT-(x)HA ceramics, respectively, indicating the disappearance of Curie point after adding HA into BCZT ceramics.

3.4.2 Ferroelectric properties

The field-dependent polarization (P-E) hysteresis loops of the (100-x)BCZT-(x)HA composites measured at room temperature with a summary of saturation and remanent polarizations (P_{sat} and P_r, respectively) are presented in Figure 6. It can be seen in Figure 6(a) that the evolution of polarization reversal or domain switching as a function of applied field was observed in the pure BCZT ceramic, indicating the essential characteristic of ferroelectric materials. However, the addition of non-ferroelectric HA into BCZT caused a huge drop of ferroelectric properties as evident in the disappearance of ferroelectric P-E hysteresis loop for the (100-x)BCZT-(x)HA composites. Figure 6(b) shows that the values of P_{sat} and P_r at 30 kV·cm^{-1} reduced dramatically when introducing 10 wt% HA into BCZT ceramic, leading to the presence of $P_{sat} \sim 2.25$ μC·cm^{-2} and $P_r \sim 0.71$ μC·cm^{-2}. As HA amount further increased to 50 wt%, the lowest values of P_{sat} and P_r were observed in this composition. This can be explained by the presence of secondary phases, as discussed in section 3.1. In contrast to the BT-HA composite, the poled 90% BT-10% HA composite showed an asymmetric P-E loop at the maximum field of 2 kV·mm^{-1} (~20 kV·cm^{-1}) with remanent polarization (P_r) of 0.02 C·m^{-2} (~ 2 μC·cm^{-2}) [30]. These findings suggest that the formation of secondary phases due to the reactivity between BCZT and HA plays a crucial role in the drop of the polarization in the (1-x)BCZT-(x)HA composite compared to the observation in the BT-HA composite.

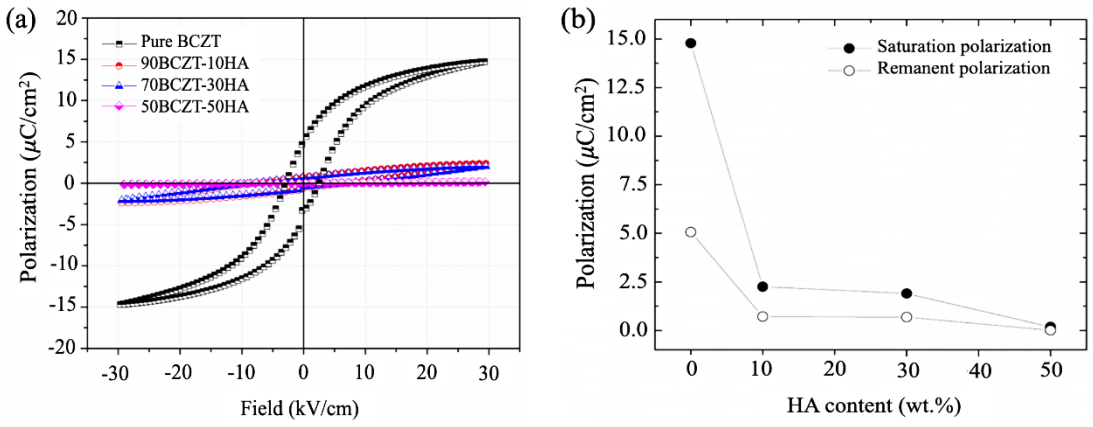

Figure 6. (a) The field-dependent polarization P-E loops for the (100-x)BCZT-(x)HA composites, and (b) the saturation and remanent polarizations as a function of HA content.

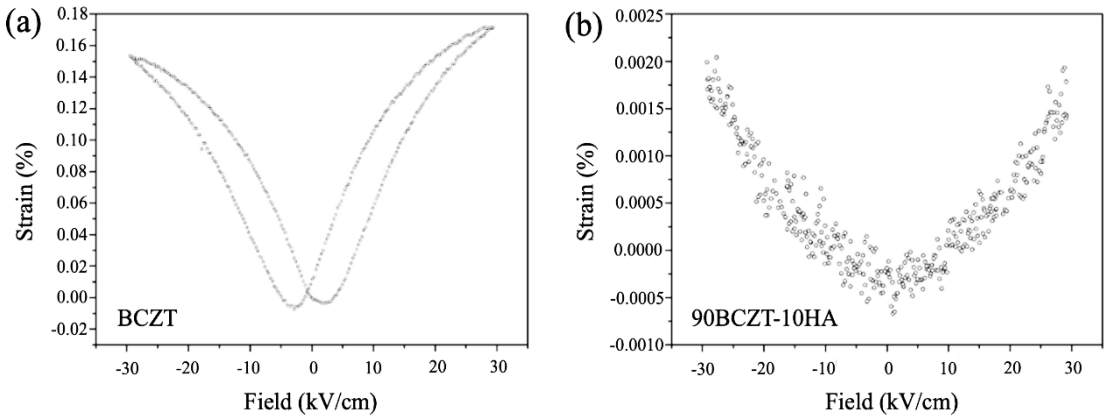

Figure 7. Strain-field plots measured at 37°C for (a) BCZT ceramic, and (b) 90BCZT-10HA ceramic.

3.4.3 Piezoelectric properties

The converse piezoelectric effect was investigated for the pure BCZT ceramic in comparison with the 90BCZT-10HA ceramic, in which the largest ε_r, P_{sat}, and P_r were observed for the (100-x)BCZT-(x)HA composites. Figure 7 illustrates the field-induced strain (s-E) butterfly loop measured at body temperature (~ 37°C). A butterfly shape of s-E curve was found for the pure BCZT ceramic with average maximum strain of ~0.16% at 30 kV·cm^{-1}. This is due to the movement and switching of non-180° domain walls, as well as changes in polarization within the crystal lattice under the application of an electric field [28]. In contrast, a linear dependence of the strain-field relationship was found in the 90BCZT-10HA ceramic, with a significant lower and noisier piezoelectric strain of ~0.0020% observed at 30 kV·cm^{-1}.

In addition, the converse piezoelectric coefficient (d_{33}) was calculated using the maximum strain divided by the given coaxial field [31]. It was found that the pure BCZT ceramic showed d_{33} of 551 pm·V^{-1}, while d_{33} of 5.94 pm·V^{-1} was observed in the 90BCZT-10HA ceramic. Additionally, Carter described that the presence of converse piezoelectric effect in the bone can be beneficial for preventing bone atrophy by enhancing mechanical stimulation on the surrounding bone, leading to the enhancement of bone formation and the decrease of bone resorption. Moreover, current information suggested that, during bone deformation from mechanical loading, osteocytes will release various signalling molecules that may have a connection to the occurrence of converse piezoelectric effect in bone [32].

3.5 Wettability

Wettability is an essential surface property that describes the interaction between bone cells and material surfaces, as well as cell adhesion and spreading on implant materials. [6,33] It is well known that a lower contact angle (θ) represents a better wettability. In other words, the surface is hydrophilic if θ < 90° and hydrophobic if θ > 90° [34]. In this work, contact angle measured on the ground surface for the unpoled (100-x)BCZT-(x)HA composites was investigated, shown in Figure 8. It was found that the highest θ of 91.7° was observed in the pure BCZT ceramic, indicating a poor wettability or hydrophobic surface. Conversely, the improvement of wetting behavior was found when adding HA into BCZT ceramics, since a slight decrease of θ (< 90°) was observed in the (100-x)BCZT-(x)HA composites. This is possibly due to the increase in porosity observed in the (100-x)BCZT-(x)HA composites, as described in section 3.3, which consequently impacted the presence of surface textures [35].

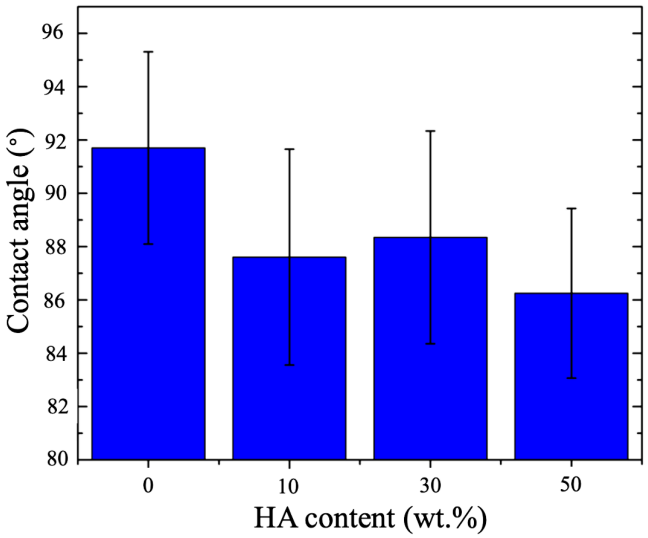

Figure 8. Comparison of contact angle for the (100-x)BCZT-(x)HA composites at different HA content.

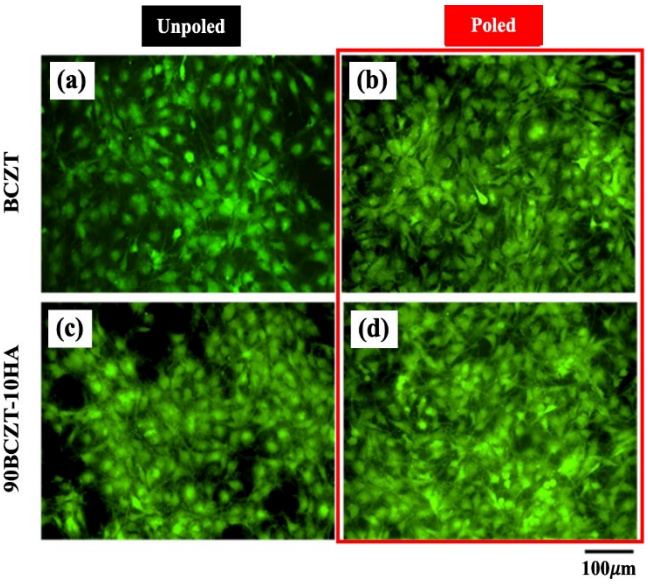

Figure 9. Live/dead assay of MC3T3-E1 cells after 24 h exposure to (a) unpoled BCZT, (b) poled BCZT, (c) unpoled 90BCZT-10HA, and (d) poled 90BCZT-10HA ceramics. Viable cells appeared with a green stain, while the dead cells had a red stain.

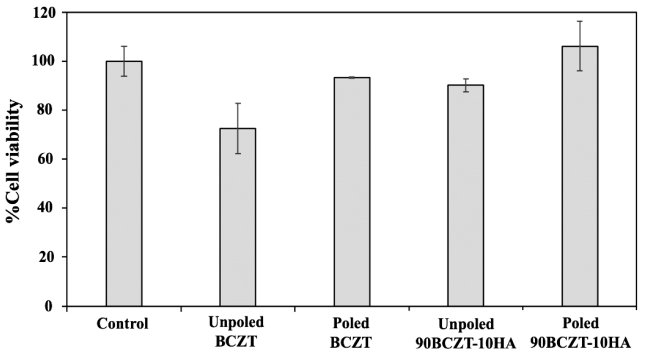

Figure 10. The viability of MC3T3-E1 cells after 24 h exposure to unpoled and poled BCZT were compared to the unpoled and poled 90BCZT-10HA ceramics. Polystyrene well was used as a control.

In this work, although the lowest contact angle (θ = 86.2°) was found in the 50BCZT-50HA composition, it showed the lowest electrical properties, as described earlier in Section 3.4. On the other hand, the addition of 10wt%HA into BCZT also caused a decrease of contact angle (θ = 87.6°) with a small difference compared to θ of the 50BCZT-50HA composition. However, the electrical properties of the 90BCZT-10HA composition were significantly higher than those observed in the 50BCZT-50HA composition. Therefore, to evaluate the impact of HA addition to the BCZT piezoceramic on the biocompatibility, the pure BCZT and the 90BCZT-10HA composition were selected for the cell viability test, as presented in the following section.

3.6 In vitro biocompatibility

The viability of MC3T3-E1 cells cultured on the unpoled and negatively poled surfaces of BCZT and 90BCZT-10HA ceramics was investigated using a live/dead assay, as shown in Figure 9. Live cells were stained green, while dead cells were stained red. After 24 h of incubation, results showed that the cells seeded on all tested ceramics stained green, indicating that both unpoled and poled BCZT and 90BCZT-10HA ceramics were non-cytotoxic. However, Vouilloz *et al.* reported that the dissolution of Ba^{2+} ions from the $Ba_3(PO_4)_2$ secondary phase played a crucial role in the presence of cytotoxicity for the BT-HA ceramic [19]. Further experiments such as cell-based toxicity assays combined with the investigation of Ba^{2+} in the cell culture solution by XRF would help to clarify the impact of Ba^{2+} release from the $Ba_3Ca_3(PO_4)_2$ and Ba_2TiO_4 secondary phases observed in the BCZT-HA ceramic on cytotoxicity and cell viability. In addition, a slight difference in cell number was observed in both unpoled and poled BCZT and 90BCZT-10HA ceramics. For morphological observation, MC3T3-E1 cells displayed a similar spread morphology in all samples.

Cell viability was also assessed after 24 h of incubation using the alamar blue assay. Figure 10 showed that cell viability surpassed 70% in all samples, indicating that all tested ceramic samples were non-cytotoxic according to ISO-10993-5: In vitro cytotoxicity tests. Interestingly, this study demonstrates for the first time that the number of viable cells observed in the poled 90BCZT-10HA ceramics is significantly higher than that observed in the unpoled BCZT ceramics. This observation is possibly due to the occurrence of negative charges on poled ceramic, which can induce the accumulation of cations (Ca^{2+}, Mg^{2+}, K^+, Na^+) on the polarized surface of the 90BCZT-10HA ceramic and consequently promote protein adsorption and cell proliferation on this surface [8]. Hence, this work found that the incorporation of 10 wt% HA into BCZT with a poling process could modify the sample properties favorable for cell adhesion and survival, leading to a promising candidate for bone-repair applications.

4. Conclusions

This work investigated the influence of HA incorporated into BCZT ceramic on the relationship between physical, electrical, and biological properties for bone-repair applications. The XRD result showed that, when introducing HA into BCZT from 10wt% to 50 wt% and sintering at 1250°C for 3 h, the reactivity between BCZT and HA was observed as evident by the presence of various secondary phases,

for examples, $CaTiO_3$, $Ba_3Ca_3(PO_4)_2$, and Ba_2TiO_4. Moreover, the SEM observation revealed that the average grain size was dropped dramatically when adding HA into BCZT. Furthermore, the addition of HA into BCZT caused a gradual decrease of densities, while porosity increased with increasing HA content. Although the electrical properties of the pure BCZT ceramic were higher than those of the 90BCZT-10HA composite, the number of viable cells found in the 90BCZT-10HA composite was greater than in the pure BCZT ceramic. Additionally, this work demonstrates for the first time that the number of viable cells observed in the poled 90BCZT-10HA ceramics was significantly higher than that observed in the unpoled BCZT ceramics. These findings suggest that the BCZT-HA composite has potential for use in bone-repair applications. Further evaluation of its biological properties could help to assess its performance in these applications.

Acknowledgment

This study was supported by Thammasat University Research Fund, Contract number TUFT050/2563. Additionally, Manita Boonchoo thanks the scholarship for talent student to study graduate program in Faculty of Science and Technology, Thammasat University, Contract number TB27/2563. We would also like to express our gratitude to Prof. Dr. Naratip Vittayakorn and Dr. Phieraya Pulphol for supporting on dielectric measurements. In addition, a constructive discussion on the results with Assoc. Prof. Dr. Wanwilai Vittayakorn and Assoc. Prof. Dr. Benya Cherdhirunkorn is acknowledged. Lastly, a sincere thank you to Mr. Gregory Alan Smith for proofreading this article.

References

[1] E. Fukuda, and I. Yasuda, "On the piezoelectric of bone," *Journal of Physical Societry of Japan*, vol. 12, pp. 1158-1162, 1957.

[2] A. B. M. Braden, I. Beider, and B.G Ritter, "Electrical and piezo-electrical properties of dental hard tissues," *Nature*, vol. 212, pp. 1565-1566, 1966.

[3] F. R. Baxter, C. R. Bowen, I. G. Turner, and A. C. Dent, "Electrically active bioceramics: a review of interfacial responses," *Annals of Biomedical Engineering*, vol. 38, no. 6, pp. 2079-2092, 2010.

[4] A. Blázquez-Castro, A. García-Cabañes, and M. Carrascosa, "Biological applications of ferroelectric materials," *Applied Physics Reviews*, vol. 5, no. 4, p. 41101, 2018.

[5] J. B. Park, A. F. v. Recum, G. H. Kenner, B. J. Kelly, W. W. Coffeen, and M. F. Grether, "Piezoelectric ceramic implants: a feasibility study," *Journal of Biomedical Materials Research*, vol. 15, pp. 103-110, 1981.

[6] K. K. Poon, M. C. Wurm, D. M. Evans, M. A. Einarsrud, R. Lutz, and J. Glaum, "Biocompatibility of (Ba,Ca)(Zr,Ti)O_3 piezoelectric ceramics for bone replacement materials," *Journal of Biomedical Materials Research Part B: Applied Biomaterials*, vol. 108, no. 4, pp. 1295-1303, 2020.

[7] W. Liu, and X. Ren, "Large piezoelectric effect in Pb-free ceramics," *Physical Review Letters*, vol. 103, no. 25, p. 257602, 2009.

[8] W. Chen, Z. Yu, J. Pang, P. Yu, G. Tan, and C. Ning, "Fabrication of biocompatible potassium sodium niobate piezoelectric ceramic as an electroactive implant," *Materials (Basel)*, vol. 10, no. 4, p. 345, 2017.

[9] J. A. Hermann-Muñoz, J. A. Rincón-López, D. A. Fernández-Benavides, R. Detsch, J.M. Alvarado-Orozco, A. R. Boccaccini, and J. Muñoz-Saldaña, "In-vitro bioactivity and cytotoxicity of polarized $(Bi_{0.5}Na_{0.5})TiO_3$ ceramics as a novel biomaterial for bone repair," *Materials Letters*, vol. 275, p. 128078, 2020.

[10] S. Nakamura, H. Takeda, and K. Yamashita, "Proton transport polarization and depolarization of hydroxyapatite ceramics," *Journal of Applied Physics*, vol. 89, no. 10, pp. 5386-5392, 2001.

[11] K. Lin, and J. Chang, "1 - Structure and properties of hydroxyapatite for biomedical applications," in *Hydroxyapatite (Hap) for Biomedical Applications*, M. Mucalo Ed.: Woodhead Publishing, 2015, pp. 3-19.

[12] S. N. T. Kobayashi, and K. Yamashita, "Enhanced osteobonding by negative surface charges of electrically polarized hydroxyapatite," *Journal of Biomedical Materials Research*, vol. 59, no. 3, pp. 477-484, 2002.

[13] T. K. M. Ohgaki, M. Katsura, and K. Yamashita, "Manipulation of selective cell adhesion and growth by surface charges of electrically polarized hydroxyapatite," *Journal of Biomedical Materials Research*, vol. 57, no. 3, pp. 366-373, 2001.

[14] S. Bodhak, S. Bose, and A. Bandyopadhyay, "Electrically polarized HAp-coated Ti: In vitro bone cell–material interactions," *Acta Biomaterialia*, vol. 6, no. 2, pp. 641-651, 2010.

[15] S. Manohar, S. K. Belliraj, S. P. Sadhu, S. K. S. Bhagavatham, S. Muthukumar, S. Venketesh, and K. Varma, "Novel Lead-free biocompatible piezoelectric Hydroxyapatite (HA) – BCZT ($Ba_{0.85}Ca_{0.15}Zr_{0.1}Ti_{0.9}O_3$) nanocrystal composites for bone regeneration," *Nanotechnology Reviews*, vol. 8, no. 1, pp. 61-78, 2019.

[16] M. Prakasam, M. Albino, E. Lebraud, M. Maglione, C. Elissalde, and A. Largeteau, "Hydroxyapatite-barium titanate piezo-composites with enhanced electrical properties," *Journal of the American Ceramic Society*, vol. 100, no. 6, pp. 2621-2631, 2017.

[17] Y. Tang, C. Wu, Z. Wu, L. Hu, W. Zhang, and K. Zhao, "Fabrication and in vitro biological properties of piezoelectric bioceramics for bone regeneration," *Scientific Reports*, vol. 7, p. 43360, 2017.

[18] T. Tariverdian, A. Behnamghader, P. Brouki Milan, H. Barzegar-Bafrooei, and M. Mozafari, "3D-printed barium strontium titanate-based piezoelectric scaffolds for bone tissue engineering," *Ceramics International*, vol. 45, no. 11, pp. 14029-14038, 2019.

[19] F. J. Vouilloz, M. S. Castro, G. E. Vargas, A. Gorustovich, and M. A. Fanovich, "Reactivity of $BaTiO_3$-$Ca_{10}(PO_4)_6(OH)_2$ phases in composite materials for biomedical applications," *Ceramics International*, vol. 43, no. 5, pp. 4212-4221, 2017.

[20] B. Ozcelik, C. Ergun, and H. Liu, "A study on calcium phosphate/barium titanate composites: phase characterization, piezoelectric property, and cytocompatibility," *Journal of the Australian Ceramic Society*, vol. 56, no. 4, pp. 1197-1216, 2020.

[21] N. Koju, P. Sikder, B. Gaihre, and B. B. S, " Smart injectable self-setting monetite based bioceramics for orthopedic applications," *Materials (Basel)*, vol. 11, no. 7, p. 1258, 2018.

[22] B. Tandon, J. J. Blaker, and S. H. Cartmell, "Piezoelectric materials as stimulatory biomedical materials and scaffolds for bone repair," *Acta Biomaterialia*, vol. 73, pp. 1-20, 2018.

[23] A. Z. Khalf, and D. A. Hall, "Influence of barium borosilicate glass on microstructure and dielectric properties of (Ba,Ca)(Zr,Ti)O_3 ceramics," *Journal of the European Ceramic Society*, vol. 38, no. 13, pp. 4422-4432, 2018.

[24] C. Chen, H. Zhuang, X. Zhu, D. Zhang, K. Zhou, and H. Yan, "Effect of Ca substitution sites on dielectric properties and relaxor behavior of Ca doped barium strontium titanate ceramics," *Journal of Materials Science: Materials in Electronics*, vol. 26, no. 4, pp. 2486-2492, 2015.

[25] D. E. Newbury, "Mistakes encountered during automatic peak identification of minor and trace constituents in electron-excited energy dispersive X-ray microanalysis," *Scanning*, vol. 31, no. 3, pp. 91-101, 2009.

[26] L. E. Cross, "Relaxor ferroelectrics," *Ferroelectrics*, vol. 76, no. 1, pp. 241-267,1987.

[27] D. Khare, B. Basu, and A. K. Dubey, "Electrical stimulation and piezoelectric biomaterials for bone tissue engineering applications," *Biomaterials*, vol. 258, p. 120280, 2020.

[28] D. Damjanovic, "Ferroelectric, dielectric and piezoelectric properties of ferroelectric thin films and ceramics," *Reports on Progress in Physics*, vol. 61, no. 9, pp. 1267-1324, 1998.

[29] K. H. Härdtl, "Electrical and mechanical losses in ferroelectric ceramics," *Ceramics International*, vol. 8, no. 4, pp. 121-127, 1982.

[30] F. R. Baxter, I. G. Turner, C. R. Bowen, J. P. Gittings, and J. B. Chaudhuri, "An in vitro study of electrically active hydroxyapatite-barium titanate ceramics using Saos-2 cells," *Journal of Materials Science: Materials in Medicine*, vol. 20, no. 8, pp. 1697-708, 2009.

[31] J. Rödel, W. Jo, K. T. P. Seifert, E.-M. Anton, T. Granzow, and D. Damjanovic, "Perspective on the development of lead-free piezoceramics," *Journal of the American Ceramic Society*, vol. 92, no. 6, pp. 1153-1177, 2009.

[32] A. Carter, K. Popowski, K. Cheng, A. Greenbaum, F. S. Ligler, and A. Moatti, "Enhancement of bone regeneration through the converse piezoelectric effect, a novel approach for applying mechanical stimulation," *Bioelectricity*, vol. 3, no. 4, pp. 255-271, 2021.

[33] S. Lavenus, P. Pilet, J. Guicheux, P. Weiss, G. Louarn, and P. Layrolle, "Behaviour of mesenchymal stem cells, fibroblasts and osteoblasts on smooth surfaces," *Acta Biomaterialia*, vol. 7, no. 4, pp. 1525-1534, 2011.

[34] A. W. Adamson, Physical Chemistry of Surfaces, 6th Edition ed. Wiley, 1997, p. 808.

[35] S. R. Paital, and N. B. Dahotre, "Wettability and kinetics of hydroxyapatite precipitation on a laser-textured Ca-P bioceramic coating," *Acta Biomaterialia*, vol. 5, no. 7, pp. 2763-72, 2009.